

AperTO - Archivio Istituzionale Open Access dell'Università di Torino

Rationally designed hyaluronic acid-based nano-complexes for pentamidine delivery

This is a pre print version of the following article:

Original Citation:

Availability:

This version is available <http://hdl.handle.net/2318/1720945> since 2019-12-30T17:22:28Z

Published version:

DOI:10.1016/j.ijpharm.2019.118526

Terms of use:

Open Access

Anyone can freely access the full text of works made available as "Open Access". Works made available under a Creative Commons license can be used according to the terms and conditions of said license. Use of all other works requires consent of the right holder (author or publisher) if not exempted from copyright protection by the applicable law.

(Article begins on next page)

Rationally designed hyaluronic acid-based nano-complexes for pentamidine delivery

Flavia Carton^{1,2}, Yves Chevalier¹, Letizia Nicoletti^{1,3}, Małgorzata Tarnowska¹, Barbara Stella³, Silvia Arpicco³, Manuela Malatesta², Lars Petter Jordheim⁴, Stéphanie Briançon¹, and Giovanna Lollo^{1}*

¹University of Lyon, Université Claude Bernard Lyon 1, CNRS, LAGEPP UMR 5007, 43 bd 11 Novembre 1918, 69622, Villeurbanne, France.

²Department of Neurosciences, Biomedicine and Movement Sciences, Anatomy and Histology Section, University of Verona, Strada le Grazie 8, Verona, Italy.

³Department of Drug Science and Technology, University of Torino, Via P. Giuria 9, Torino, Italy.

⁴University of Lyon, Université Claude Bernard Lyon 1, INSERM 1052, CNRS 5286, Centre Léon Bérard, Centre de Recherche en Cancérologie de Lyon, 69008 Lyon, France.

Keywords: hyaluronic acid, polyarginine, pentamidine, biomaterials, drug delivery systems;

***Corresponding Author**

***E-mail: giovanna.lollo@univ-lyon1.fr**

19 **Abstract**

20 Nanoparticles of polymeric complexes made of hyaluronic acid and polyarginine were investigated
21 for the encapsulation of the cationic hydrophilic drug pentamidine isethionate. The interaction
22 between the anionic hyaluronic acid and the cationic pentamidine and the formation of polyelectrolyte
23 complexes of them were firstly studied. Then, nanoparticles made of mixed hyaluronic acid /
24 polyarginine loaded with pentamidine were developed as drug delivery systems. A monodisperse
25 population of negatively charged pentamidine- loaded nanoparticles allowed high encapsulation rates
26 of pentamidine (80%). Such high encapsulation efficiency coming from ion exchange was confirmed
27 by measurements of the counterion isethionate released from pentamidine during nanoparticles
28 formation. Besides, freeze-dried pentamidine-loaded nanoparticles kept their integrity after their
29 reconstitution in water. *In vitro* studies on human lung (A549) and breast (MDA-MB-231) cancer cell
30 lines showed that pentamidine-loaded nanoparticles were more cytotoxic in comparison to the free
31 drug, suggesting an enhanced internalization of encapsulated drug by cancer cells.

33 **1. Introduction**

34 Delivery of hydrophilic drugs is a challenge owing to their difficult crossing through cells walls that
35 limits their therapeutic activity. Encapsulation is often required in order to enhance drug
36 bioavailability. In case of ionic drugs, complexation with polyelectrolytes of opposite charge is a
37 suitable methodology as it has been extensively studied for transfection of DNA and siRNA^{1,2}. Upon
38 formation of a charge-stoichiometric complex, the neutral species may undergo precipitation as
39 nanoparticles, resulting in drug encapsulation inside a nanocarrier. Electrostatic interaction is one of
40 the driving forces for such complexation. However, electrostatic binding often occurs by an ion
41 exchange process such that the overall charge balance is null. Non-electrostatic interactions also
42 matter, so that each system deserves a specific investigation aiming at better mastery over the
43 encapsulation process.

Over the last decades, the development of pharmaceutical nanocarriers based on natural polysaccharides aroused a growing interest in drug delivery technologies based on ionic complexation³. Natural polysaccharides have interesting properties as biocompatibility, biodegradability and low toxicity suitable for biomedical applications⁴⁻⁶. Besides, they bear a large variety of reactive groups, a wide range of molar masses (M_w), varying chemical compositions and origins, which make them a versatile biomaterial for the preparation of nanometric carriers⁷.

Among the different natural polysaccharides, hyaluronic acid (HA) has been widely used in the pharmaceutical field because of its interesting physicochemical and biological properties^{8,9}. HA belongs to the class of anionic glycosaminoglycans (GAGs) formed by several identical subunits (D-glucuronic acid and N-acetyl-D-glucosamine disaccharide) bound together by β -1,4 and β -1,3 glycosidic bonds^{10,11}. HA is an important component of the extracellular matrix (ECM) highly distributed throughout connective, epithelial, and neural tissues in which plays essential physiological roles⁸. HA backbone itself is endowed with targeting moieties that specifically recognize and interact with different cell surface proteins like stabilin-2, RHAMM, lymphatic vessel endothelial hyaluronan receptor 1 (LYVE-1), and CD44. Also, low molecular weight HA regulates Toll Like Receptor (TRL). Among all these receptors, CD44 represent the most studied HA-receptors in inflammation and tumor pathologies¹²⁻¹⁴.

Therefore, specific targeting of these receptors has been exploited as an effective strategy for increasing accumulation of associated drug at the target site^{15,16}. In addition, HA bears a carboxylic group in each glucuronic unit (pKa 3-4) which provides an acidic polyelectrolyte character enabling interactions with cationic polymers or molecules possessing appropriate basic groups for formation of complexes¹⁷.

So far, exploitation of HA properties to polymeric conjugates, liposomes, microparticles, and nanoparticles have been attempted. Such dosage forms are generally obtained through formation of self-assembling micelles, chemical conjugation via cross-linking approaches or ionic gelation¹⁷⁻²⁰. Among these techniques, polyelectrolyte complexation represents the most widely used method to

tailor HA-based drug delivery systems, because of the mild processing conditions, absence of organic solvents and wide range of cationic polymers undergoing interactions with HA²¹. Several previous works disclosed instances showing the ability of HA-based polyelectrolyte nanostructures to associate active compounds such as genetic materials or positively charged drugs⁹. Contreras-Ruiz et al. described nanoparticles made of HA complexed with chitosan (CS) oligomers for pDNA delivery. HA-CS complexes entered cells and yielded significant transfection of pDNA into the corneal and conjunctival cells²². Recently, a novel ionic metal complex based on HA and an oxaliplatin derivative, dichloro(1,2-diaminocyclohexane)platinum(II) (DACHPt), has been patented. Compared to the DACHPt aqueous solution injected intravenously, DACHPt-loaded nano-complexes protected the associated drug from enzymatic degradation, thereby enhancing plasmatic concentration while lowering drug elimination rate²³. Also, Battistini et al. reported a doxorubicin-HA ionic complex as a tumor targeting drug delivery system. *In vitro* studies on tumor cells overexpressing CD44 receptors demonstrated the improved internalization of the complexes in comparison to the free drug¹⁵. Based on this background information, the present work deals with an extensive physicochemical characterization of polyelectrolyte complexes (PECs) made of HA and a cationic molecule, pentamidine isethionate (PTM) as model drug. PTM is well known for its antiprotozoal, antifungal and anticancer activity^{24,25}. It is a water-soluble molecule with two terminal amidine groups, protonated in a wide pH range ($pK_a = 12-13$) including physiological/neutral conditions. To stabilize PTM-HA PECs and maximize the amount of associated PTM, polyarginine (PArg) was used to crosslink HA and form nanoparticles (NPs)¹³. PArg is a biocompatible cationic poly(aminoacid) belonging to the cell-penetrating peptide polymers able to improve intracellular delivery of therapeutic agents²⁶. At neutral pH, the amine groups of PArg are protonated and interact with carboxylic moieties of HA, leading to the formation of NPs. Also, polyion complexes made of HA and protamine, have been described developed for the encapsulation of different active compounds^{27,28}. In the current work, the formation of PECs made of HA and PTM and NPs made of HA and PArg were investigated by studying size and zeta potential of NPs and quantifying the amount of

isethionate, the PTM counterion, released during the formation process while varying the relative concentrations of the PECs-forming components. Lyophilization studies were also carried out in order to ensure preservation of pentamidine-loaded nanoparticles (PTM-loaded NPs) as a dry form upon long-term storage. The morphology of the formed particles was analyzed by transmission electron microscopy (TEM) and cryogenic-transmission electron microscopy (Cryo-TEM). Finally, *in vitro* studies were performed on lung and breast human cell lines (A549 and MDA-MB 231) to assess the anticancer activity of encapsulated PTM.

2. Experimental section

2.1. Materials

Sodium hyaluronate (HA) (weight-average molar mass, $M_w = 3.9 \cdot 10^4 \text{ g} \cdot \text{mol}^{-1}$) was purchased from LifeCore[®] Biomedical (Chaska, Minnesota, USA). Poly (L-arginine hydrochloride) (PArg) (weight-average molar mass, $M_w = 5.8 \cdot 10^3 \text{ g} \cdot \text{mol}^{-1}$) was purchased from Alamanda[®] Polymers (Huntsville, Alabama, USA) and pentamidine isethionate (PTM) (molar mass, $M_{\text{mol}} = 592.679 \text{ g} \cdot \text{mol}^{-1}$) from Sigma-Aldrich[®] (St Quentin-Fallavier, France). Milli-Q water was obtained using a milli-Q Academic System (Merck Millipore[®], St Quentin-Fallavier, France). Sodium silicotungstate used for staining in TEM was supplied from Agar Scientific (Parsonage Lane, Stansted, UK). Dulbecco's Modified Eagle Medium (DMEM) without glucose, glutamine, phenol red and sodium pyruvate was bought from Gibco[®] (Thermo Fisher Scientific[®], Waltham, Massachusetts, USA) and used to evaluate the stability in physiological medium. Human lung carcinoma cells (A549) and human breast adenocarcinoma cells (MDA-MB-231) were from ATCC and grown in complete Dulbecco's Modified Eagle Medium (DMEM) supplemented with 10% fetal bovine serum (Thermo Fisher Scientific[®]), 100 U/mL penicillin (Thermo Fisher Scientific[®]), $100 \text{ mg} \cdot \text{mL}^{-1}$ streptomycin (Thermo Fisher Scientific[®]) and 1% L-glutamine (Life Technologies). 3-(4,5-dimethylthiazol-2-yl)-2,5-diphenyltetrazolium bromide (MTT) was purchased from Sigma-Aldrich (St Quentin-Fallavier, France).

2.2. Solubility study of pentamidine

Saturated solutions of PTM at different pH (pH 7.4, 9, 10, 12) and in phosphate buffer saline (PBS, pH 7.4) were prepared. The solutions were stirred for 2 h at room temperature and left overnight to reach equilibrium. Then, all samples were centrifuged (62.000 g, 30 min, 20 °C) and the supernatant was analyzed for PTM by measuring its UV absorbance at 270 nm (UV-1280, Shimadzu, Marne-la-Vallée, France).

2.3. Preparation of pentamidine-hyaluronic acid polyelectrolyte complexes

Pentamidine-hyaluronic acid polyelectrolyte complexes (PTM-HA PECs) were prepared by mixing aqueous solutions of PTM and HA at different PTM/HA mole ratios ranging between 0.2 and 2.4. Seven different PTM-HA PECs were obtained by adding 0.5 mL of HA aqueous solution (2.5 mg·mL⁻¹) into 0.5 mL of PTM aqueous solution of concentrations ranging from 0.6 to 9 mg·mL⁻¹. Size, polydispersity index, electrophoretic mobility and pH of PECs were studied.

2.4. Preparation of blank and pentamidine-loaded nanoparticles

Blank nanoparticles (HA-PArg NPs) were prepared by polyelectrolyte complexation using a similar methodology of ionic gelation²⁹. Briefly, 0.5 mL of an anionic HA solution at different concentrations ranging from 1.25 to 5.00 mg·mL⁻¹ were added to an equal volume of solution containing cationic polyarginine (PArg) (0.27 mg·mL⁻¹). Nine different formulations with HA/PArg mole ratio between 0.82 to 8.25 were prepared.

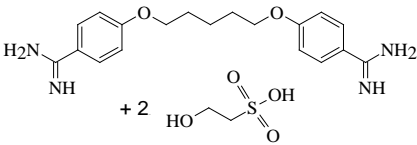
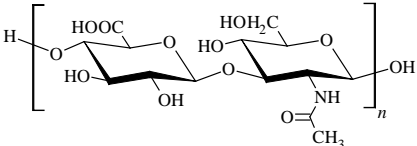
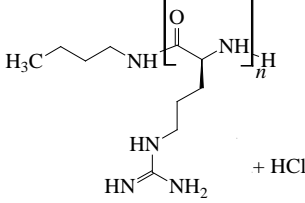
Pentamidine-loaded nanoparticles (PTM-loaded NPs) were obtained by mixing 0.5 mL of aqueous solution of PTM at concentrations ranging from 0.50 to 0.17 mg·mL⁻¹ and 0.5 mL of cationic PArg solution at 0.18 mg·mL⁻¹. This premix was left under agitation during 10 min, and 0.5 mL of HA solution of concentrations ranging from 0.83 to 3.3 mg·mL⁻¹ were added. The mole ratio between HA (negatively charged) and PArg plus PTM (both positively charged) was ranging between 1.13 and

148 4.51. HA-PArg NPs and PTM-loaded NPs were characterized in terms of pH, size, polydispersity
 149 index, zeta potential and encapsulation efficiency. The main characteristics of all the compounds used
 150 to obtain PECs and NPs are listed in Table 1.

151

152

153 **Table 1.** Chemical characteristics of the compounds used to obtain polyelectrolyte complexes and
 154 nanoparticles. The molar masses given for polymers are that of their repeat unit.

Compound	Molecular Formula	Molecular structure	pKa	M_w (g·mol ⁻¹)
Pentamidine isethionate	C ₂₃ H ₃₆ N ₄ O ₁₀ S ₂		12.13	592.7
Sodium Hyaluronate	(C ₁₄ H ₂₀ NO ₁₁ Na) _n		2.87	3.9·10 ⁴
Poly(L-arginine hydrochloride)	(C ₆ H ₁₄ N ₄ O ₂) _n		12.42	5.8·10 ³

155

156

157 2.5. Physicochemical characterization of polyelectrolyte complexes, blank and pentamidine- 158 loaded nanoparticles

159 Size distribution and surface potential of the prepared particles (PECs and NPs) were analyzed using
 160 a Malvern Zetasizer® (model Nano ZS, Malvern Panalytical, Malvern, UK). Particle size distributions
 161 were determined by Dynamic Light Scattering (DLS) of samples diluted with milli-Q water. Analyses

were carried out at 25 °C with a scattering angle of 173°. Particle size distribution was determined using the cumulants method that provides the *z*-average diameter and the polydispersity index (*PdI*). The zeta potential (ζ) was determined from the electrophoretic mobility (u_E) (Equation 1). For all measurements, samples were diluted in milli-Q water and placed in a U-shaped fold capillary cell (DTS1070) made of polystyrene and containing two electrodes of gold-plated beryllium/copper (Malvern). ζ potential was calculated according to the Henry Equation under the Smoluchowski approximation of the Henry factor $f(\kappa a)$:

$$u_E = \frac{2}{3} \frac{\varepsilon_0 \varepsilon \zeta}{\eta} f(\kappa a) \quad (1)$$

where η is the viscosity of water ($\eta = 0.887$ mPa·s at 25 °C), κ is the inverse Debye length, a is the radius of particles, and $f(\kappa a) = 3/2$.

Turbidity of PECs was monitored by absorbance measurements at 600 nm using an UV spectrometer (UV-1280 from Shimadzu, Marne-la-Vallée, France) equipped with a cuvette with an optical path of 10 mm. The turbidity (τ) was calculated from the absorbance (*Abs*) reading as $\tau = \ln(10) Abs = 2.3 Abs$.

176

2.6. Ion-exchange chromatography

Isethionate ions released due to association of positively charged PTM to negatively charged HA were quantified using ion exchange chromatography (IC) (930 Compact IC Flex, Metrohm, Switzerland) equipped with a chemical suppressor and conductivity detection. PTM-loaded NPs were centrifuged (7.000 g, 30 min, 25 °C) using Amicon® filter (Amicon Ultra-0.5, 30.000 NMWL, Millipore, Darmstadt, Germany), supernatants were recovered and injected into the IC. The analyses were conducted using Metrosep a Supp 5 250/4.0 column with an adequate pre-column at a temperature of 30 °C. For the detection of anions, the mobile phase was 8 mmol·L⁻¹ solution of Na₂CO₃ (Fischer Scientific, Illkirch, France) prepared in ultrapure water (resistivity > 18 MΩ·cm), filtered at 0.45 µm and degassed in an ultrasonic bath prior to use. The flow rate was 0.7 mL·min⁻¹.

187 Such conditions ensured linearity of calibration curve in a range from 0.005 to 5 mmol·L⁻¹ of
188 isethionate concentration.

189

190

191 **2.7. Morphology of blank and loaded nanoparticles using transmission and cryogenic** 192 **electron microscopy**

193 Transmission electron microscopy (TEM) was performed with a Philips CM120 microscope at
194 “Centre Technologique des Microstructures” (CTμ) at the University of Lyon 1 (Villeurbanne,
195 France). A small drop of suspension (5 μL) was deposited on a carbon/formvar microscope grid
196 (Delta Microscopies, Saint-Ybars, France), stained with a 1% w/w sodium silicotungstate aqueous
197 solution, and slowly dried in open air. The dry samples were observed by TEM under 120 kV
198 acceleration voltage.

199 Regarding cryogenic-transmission electron microscopy (Cryo-TEM), diluted samples of HA-PArg
200 NPs and PTM-loaded NPs were dropped onto 300 mesh holey carbon films (Quantifoil R2/1) and
201 quench-frozen in liquid ethane using a cryo-plunge workstation (made at Laboratoire de Physique
202 des Solides-LPS Orsay, France). The specimens were then mounted on a precooled Gatan 626
203 specimen holder, transferred in the microscope (Phillips CM120) and observed at an accelerating
204 voltage of 120 kV.

205

206 **2.8. Association efficiency and loading capacity of pentamidine into nanoparticles**

207 The association efficiency (AE) of PTM into loaded NPs was determined using an indirect method
208 by measurements of the concentration of free PTM in the aqueous phase. PTM-loaded NPs were
209 centrifuged (7.000 g, 30 min, 25 °C) using Amicon[®] filter (Amicon Ultra-0.5, 30.000 NMWL, Merck
210 Millipore[®], Burlington, Massachusetts, USA), supernatants were recovered and analyzed for free
211 PTM using UV absorbance at 270 nm. Calibration was performed using PTM solutions at different

concentrations from 2.5 µg·mL⁻¹ to 30 µg·mL⁻¹. From the AE values, the loading capacity (LC) of PTM-loaded NPs was calculated using the following Equations 2 and 3 respectively:

$$AE(\%) = \frac{\text{Total drug} - \text{Free drug in supernatant}}{\text{Total drug}} \times 100 \quad (2)$$

$$LC(\%) = \frac{\text{Mass of associated drug}}{\text{Mass of nanoparticles}} \times 100 \quad (3)$$

All measurements were performed in triplicate using PTM aqueous solution as control.

2.9. Stability studies of blank and pentamidine-loaded nanoparticles

Colloidal stability of HA-PArg NPs and PTM-loaded NPs was evaluated over 4 weeks under storage at 4 °C. Size, polydispersity index and ζ potential was analyzed every week. Leakage of the drug was also evaluated at the end of the storage period. The stability in DMEM without glucose, glutamine, phenol red and sodium pyruvate was tested to check the effect of protein factors on NPs aggregation.

2.10. *In vitro* release study of pentamidine-loaded nanoparticles

In vitro release behavior of PTM-loaded NPs in simulated physiological conditions (PBS at 37 °C) was performed using a bicompartamental diffusion device (Franz[®] cells) mounted with a semi-synthetic cellulose membrane (6-8 kDa MWCO from Spectra/Por, Spectrum Laboratories, The Netherlands). To ensure sink condition, 2 mL of PTM-loaded NPs prepared using 2.3 and 3.3 mg·mL⁻¹ of HA and 0.50 mg·mL⁻¹ of PTM were placed in the upper part of the cell (donor chamber). The lower part of the cell (receptor chamber) was filled with 10 mL of release media (PBS, pH 7.4 at 37 °C) with a horizontal shaking. At different time points (15 min, 30 min, 1 h, 2 h, 3 h, 4 h, 6 h, 8 h, 24 h, 48 h, 72 h), 1 mL of each sample was collected and analyzed for PTM using UV absorption (at 270 nm). The amount of drug released over time was calculated from the difference between the

236 initial total amount of the drug present in PTM-loaded NPs and the amount of PTM present in the
237 receptor chamber. The experiments were performed for both NPs in triplicate.

238

239 **2.11. Freeze-drying studies of blank and loaded pentamidine nanoparticles**

240 Once the development of NPs has been completed, HA-PArg NPs and PTM-loaded NPs were freeze-
241 dried using CRYONEXT pilot freeze dryer (Cryotec, Saint-Gély-du-Fesc, France). During the
242 formulation step, the bulking agent mannitol was added to the formulations at different concentration
243 (5%, 10% w/v). The freeze-drying program consisted of an initial freezing at -20 °C in a freezer for
244 12 h. After that, the freeze-dryer was pre-cooled at -20 °C and samples were introduced therein. Then,
245 the temperature was decreased to -50 °C at a rate of 1 °C·min⁻¹ and this temperature was kept for
246 12 h. The sublimation step was carried out at a temperature between -35 °C and 5 °C and a pressure
247 between 0.100 and 0.3000 mbar according to the recipe. Finally, a secondary drying step was carried
248 out at 35 °C and 0.010 mbar. After freeze-drying, HA-PArg NPs and PTM-loaded NPs were
249 resuspended in 1 mL of milli-Q water and left under magnetic stirring for 30 min. Size, polydispersity
250 and association efficiency of nanoparticles were measured before and after resuspension. Also,
251 morphological observations using TEM were performed.

252

253 **2.12. *In vitro* cell viability studies**

254 Human lung carcinoma cells (A549) and human breast adenocarcinoma cells (MDA-MB-231) were
255 used to evaluate the cell viability. Cells (3000 cells/well) were seeded in 96 well plates in 100 µL
256 media and left to adhere for 24 h. Then, the medium was replaced with a fresh one containing different
257 concentrations (0.01-100 µM) of free PTM, HA-PArg NPs and PTM-loaded NPs. After 72 h of
258 exposure, metabolically active cells were quantified by 3-(4,5-dimethylthiazol-2-yl)-2,5-
259 diphenyltetrazolium bromide (MTT) assay according to the supplier's instructions. Briefly, 20 µL of
260 MTT reagent (5 mg·mL⁻¹) was added in each well and the plate was incubated at 37 °C for 2 h. After
261 that the supernatant was replaced by 100 µL of isopropanol/HCl/H₂O (90/1/9 v/v/v) and the optical

density was measured at 540 nm for purple intensity and at 690 nm for the subtraction of background using a multiwell-scanning spectrophotometer (Multiskan Ascent, Labsystems SA, Cergy-pontoise, France). Cell viability from the absorbance values was calculated using the following Equation 4:

$$\text{Cell viability (\%)} = \frac{Abs_{treated}}{Abs_{untreated}} \times 100 \quad (4)$$

IC50 values were determined using the CompuSyn software.

3. Results and discussion

3.1. Solubility of pentamidine at different pH

PTM isethionate is a synthetic amidine derivative, highly soluble in water ($> 30 \text{ mg}\cdot\text{mL}^{-1}$) having a pK_a of 12.5. Its solubility was above $30 \text{ mg}\cdot\text{mL}^{-1}$ in the pH range from 3 to 10 due to the ionization of amidine groups, while at pH values higher than 12 the solubility was drastically reduced ($6.5 \text{ mg}\cdot\text{mL}^{-1}$) (Figure 1). Solubility also depended on ionic strength as the solubility of PTM in PBS pH 7.4 was around $6.9 \text{ mg}\cdot\text{mL}^{-1}$. This decrease of PTM solubility could be due to an increase of inert ions in the medium that shields the interactions between the counter-ions.

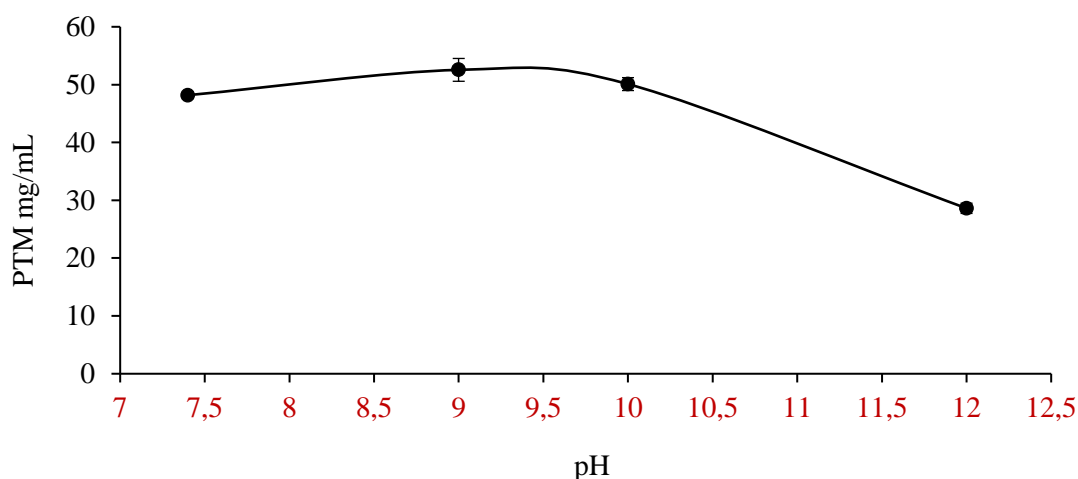


Figure 1. Solubility of PTM in aqueous media of different pH values.

3.2. Preparation and physicochemical characterization of pentamidine-hyaluronic acid polyelectrolyte

281 Polyelectrolyte complexes (PECs) are defined as complexes formed through electrostatic interactions
 282 between oppositely charged structures. The formation of PTM-HA PECs was based on the
 283 electrostatic interaction between the positively charged drug PTM containing two guanidine groups,
 284 and the negatively charged polysaccharide HA which contains one carboxylic group for each repeat
 285 unit made of two sugar residues, neutral N-acetyl-D-glucosamine and negatively charged sodium salt
 286 of D-glucuronic acid as defined in Table 1.

287 The stoichiometry of the complex was defined as the PTM/HA mole ratio of PTM molecules to HA
 288 repeat units. Different PTM-HA PECs having a mole ratio PTM/HA between 0.2 and 2.4 and the
 289 mass ratio from 0.24 to 3.6 (PEC A - PEC G) were obtained (Table 2). HA solution was added to an
 290 equal volume of PTM at different concentration under magnetic stirring. Since the concentration of
 291 the low molar mass electrolyte strongly affects the formation of the complexes, only the amount of
 292 PTM was varied³⁰.

293 All the formulations were prepared at pH values around 6-7 in order to obtain an optimal charge
 294 density that generates attractive interactions between the PTM and HA.

295

296 **Table 2.** Formulation code for PTM-HA PECs. Mole ratio, mass ratio and pH values are given.

Complexes	Mole ratio PTM/HA	Mass ratio PTM/HA	pH
PEC A	0.16	0.24	7.17
PEC B	0.34	0.5	7.07
PEC C	0.67	1.0	6.78
PEC D	0.94	1.48	6.76
PEC E	1.48	2.2	6.79
PEC F	2.01	3.0	6.65
PEC G	2.42	3.6	7.17

297

298 The concentration regime of HA solutions was devised by taking measurements of overlapping
 299 concentrations (C^*) for aqueous solution of HA of various molar masses reported by Dodero et al.³¹
 300 and extrapolating them down to the present low molar mass of HA (20 kDa). This gave $C^* =$

301 15 mg·mL⁻¹. The largest present HA concentration of 2.5 mg·mL⁻¹ was much lower than C*, showing
302 that HA concentrations were in the dilute regime.

303 DLS measurements were performed in order to study possible interactions between HA and PTM.
304 Figure 2A shows the experimental time correlation function as a function of time (at a scattering angle
305 of 173°). For all PEC solutions, the correlation function showed a trimodal profile. This distribution
306 was due to the existence of fast and slow relaxation modes in molecular motions.

307 The correlation function of the scattered amplitude $G^{(1)}(t)$ was modeled as the sum of three
308 exponential decays as in Equation 5 (Figure 2A):

309

$$310 \quad G^{(1)}(t) = A_1 e^{-\frac{t}{\tau_1}} + A_2 e^{-\frac{t}{\tau_2}} + A_3 e^{-\frac{t}{\tau_3}} \quad (5)$$

311

312 where A_i and τ_i ($i = 1, 2, 3$) are the relative scattered intensities and relaxation times for the three
313 relaxation modes respectively ($A_1 + A_2 + A_3 = 1$). The first term in the right hand side of Equation 5
314 is the fastest relaxation corresponding to the fastest motions. It was associated with the lateral
315 diffusion of isolated HA-PTM complexes characterized by a mutual diffusion coefficient D ($\tau_1^{-1} =$
316 Dq^2). The diameter of such species given by the Stokes-Einstein relationship ($D = \frac{kT}{3\pi\eta \text{Diam}}$) was 12-
317 14 nm (Figure 2B), in agreement with the expected size of a random coil of $3.9 \cdot 10^4$ g.mol⁻¹ HA. The
318 second term is a slower mode that was ascribed to associations (aggregates) of HA-PTM
319 macromolecules of mean size in the range 300-500 nm (Figure 2B). This interpretation was suggested
320 by observations of such aggregates in dilute solutions of HA reported by Maleki et al.³², and in more
321 complex systems containing HA^{33,34}. The nature of the third mode was difficult to figure out. The
322 diameter of particles that would correspond to a translational diffusion was unrealistically large
323 (~50 μm) because they were not observed by optical microscopy. The origin of this third slowest
324 relaxation might stand from slow internal motions inside HA-PTM aggregates that are not
325 translational diffusion.

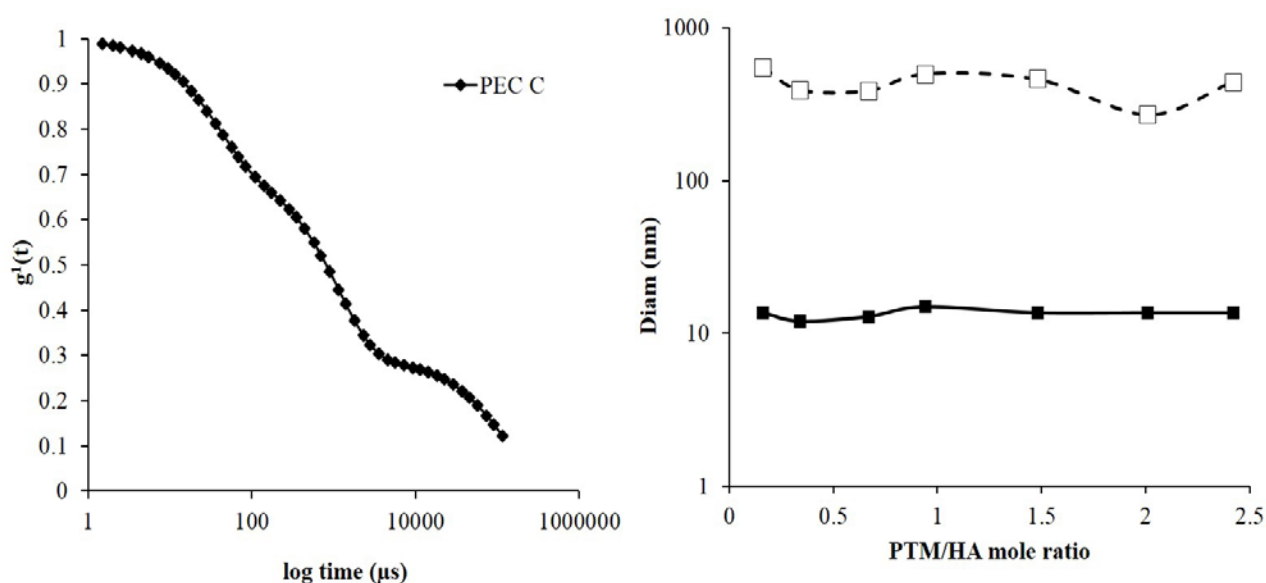
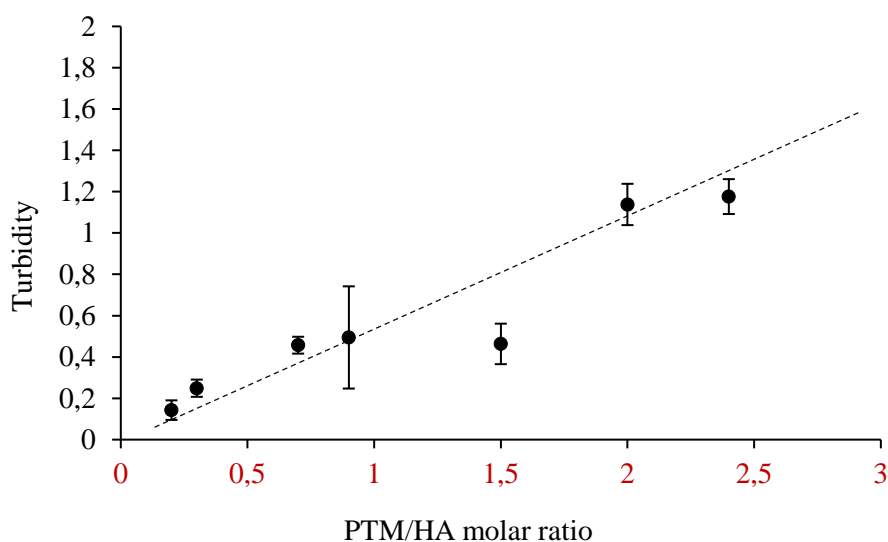


Figure 2. A) Normalized curve of correlation function ($g^1(t)$) versus time of PECs C. The curve is fitted with the aid of the Equation 5 (see text). B) Diameter (nm) of aggregated (□) and isolated (■) PEC.

Turbidity measurements of PTM-HA PECs provided a complement of the conclusions drawn from DLS (Figure 3). A slight increase of turbidity was first observed as more PTM was added to HA indicating that HA polymeric chains tended to overlap and associate each other's. As an outcome, both DLS and turbidity measurements revealed aggregation of HA as association with PTM was proceeding. The origin of such associations was probably a more hydrophobic character of the PECs as the organic PTM cations bind to HA. This provided an indirect indication for the binding of PTM to HA by means of electrostatic interaction between the two polyions.



346

347 **Figure 3.** Turbidity ($\lambda = 600$ nm) of PTM/HA PECs as a function of PTM/HA mole ratio. PEC A

348 PTM/HA = 0.2, PEC B PTM/HA = 0.3, PEC C PTM/HA = 0.7, PEC D PTM/HA = 0.9, PEC E

349 PTM/HA = 1.5, PEC F PTM/HA = 2.0, PEC G PTM/HA = 2.4. Values are given as mean \pm Sem (n

350 = 3).

351

352 Stronger binding of PTM cations than Na^+ coming from the divalent and hydrophobic natures of PTM

353 was more directly detected by measurements of electrophoretic mobility (Figure 4). Electrophoretic

354 mobility (u_E) was negative over the whole range of PTM/HA stoichiometry, progressively shifting

355 toward no mobility corresponding to electrical neutrality as increasing the concentration of PTM.

356 Electrophoretic mobility experiments clearly indicated an increase of complexation at high PTM/HA

357 mole ratio.

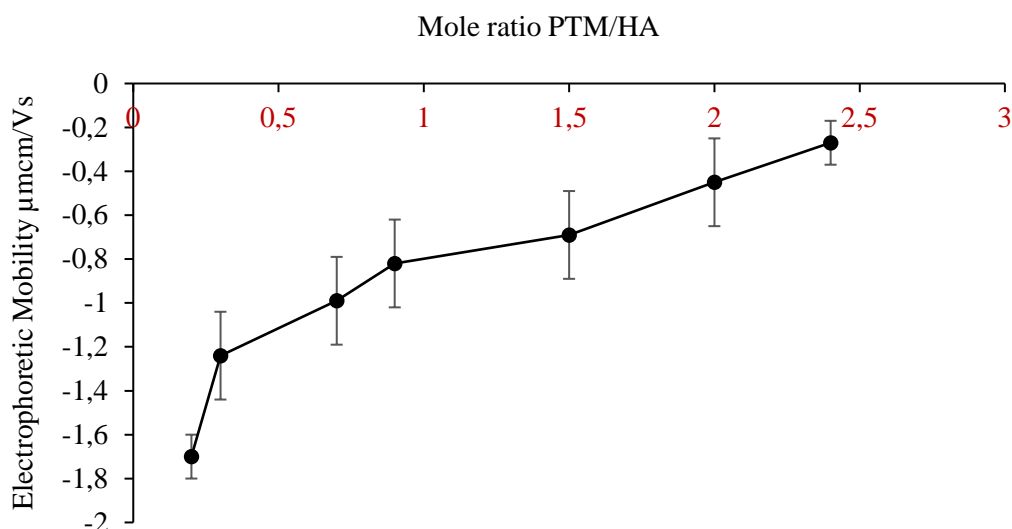


Figure 4. Electrophoretic mobility (u_E) of PTM-HA PECs in function of mole ratio PTM/HA (from 0.24 to 2.4). Values are given as mean \pm *Sem* ($n = 3$).

As an overall outcome, the conformation of the polymeric chain, turbidity and electrophoretic mobility measurements, confirmed the complexation of PTM by HA. Moreover, the electrostatic binding of PTM to HA was weak because the PTM cation was only divalent. Since the association of polyelectrolytes of opposite charges is usually quite strong, a cationic polyelectrolyte (polyarginine, PArg) was added in order to help at precipitation of nanoparticles and improve the encapsulation of PTM.

3.3. Preparation and physicochemical characterization of the blank hyaluronic acid-polyarginine nanoparticles

To enhance the formation of NPs, the cationic poly(aminoacid) PArg was used as a cross-linking agent causing the formation of insoluble PECs and thereby allowing for the formation of nanoparticles. HA-PArg NPs were prepared by polyelectrolyte complexation in a similar manner as described by Oyarzun-Ampuero et al.²⁹ Five hundred microliters of a solution containing HA at different concentrations (from 1.25 to 5 mg·mL⁻¹) were added to an aqueous solution of PArg

(0.27 mg·mL⁻¹) under magnetic stirring at room temperature for 30 min. The formation of NPs was ensured by the electrostatic interaction between the positively charged groups of PArg and the negatively charged carboxylate groups of HA. All the different formulations of HA-PArg NPs (Blank A - Blank I) were studied for their size, polydispersity index (*PdI*) and ζ potential (Table 3). The average size of the resulting blank NPs ranged between 112 and 244 nm with a low polydispersity index (*PdI* < 0.2). Values of ζ potential ranged from +33 to -22 mV. When the charge ratio HA/PArg was lower than 1.24, NPs had a size around 120 nm with a positive ζ value (+33 mV), indicating that the charge brought about by PArg was larger than that of HA. At mole ratio higher than 1.24, NPs size increased from 166 to 244 nm, and an inversion of ζ potential to -31 mV occurred. The increase in the hydrodynamic size was correlated to the amount of HA used to obtain the NPs. Besides, inversion of surface potential indicated a conformational change which exposes carboxylic groups of HA in excess with respect to cationic groups of PArg towards the external surface of NPs. Globally, the HA/PArg interaction allows the preparation of NPs of 100-250 nm size with a narrow size distribution and reversal of the electrical charge according to the charge ratio of the two polymers.

Table 3. Physicochemical characteristics of HA-PArg NPs. *PdI*: Polydispersity index. Values are given as mean \pm *Sem* (*n* \geq 3).

	Mass ratio [HA/PArg]	Mole ratio [HA/PArg]	Size (nm)	<i>PdI</i>	Zeta potential (mV)
Blank A	0.50: 0.27	0.82	112 \pm 6	< 0.2	+ 33 \pm 5
Blank B	0.75: 0.27	1.24	129 \pm 1	< 0.2	+ 32 \pm 3
Blank C	1.25: 0.27	2.06	166 \pm 7	< 0.2	- 31 \pm 1
Blank D	1.5: 0.27	2.47	158 \pm 4	< 0.2	- 38 \pm 2
Blank E	2.0: 0.27	3.30	167 \pm 3	< 0.1	- 33 \pm 2
Blank F	2.5: 0.27	4.12	180 \pm 14	< 0.1	- 29 \pm 3
Blank G	3: 0.27	4.95	201 \pm 14	< 0.1	- 31 \pm 3
Blank H	3.5: 0.27	5.77	222 \pm 11	< 0.2	- 30 \pm 4
Blank I	5: 0.27	8.25	244 \pm 5	< 0.1	- 22 \pm 3

3.4. Development and physicochemical characterization of pentamidine-loaded hyaluronic acid-polyarginine nanoparticles

PTM-loaded NPs were prepared following the protocol described for blank NPs. Different concentrations of HA ($0.83 \text{ mg} \cdot \text{mL}^{-1}$ to $3.3 \text{ mg} \cdot \text{mL}^{-1}$) were added to an aqueous solution containing PArg ($0.18 \text{ mg} \cdot \text{mL}^{-1}$) and PTM of concentration ranging from 0.5 to $0.17 \text{ mg} \cdot \text{mL}^{-1}$ (Figure 5).

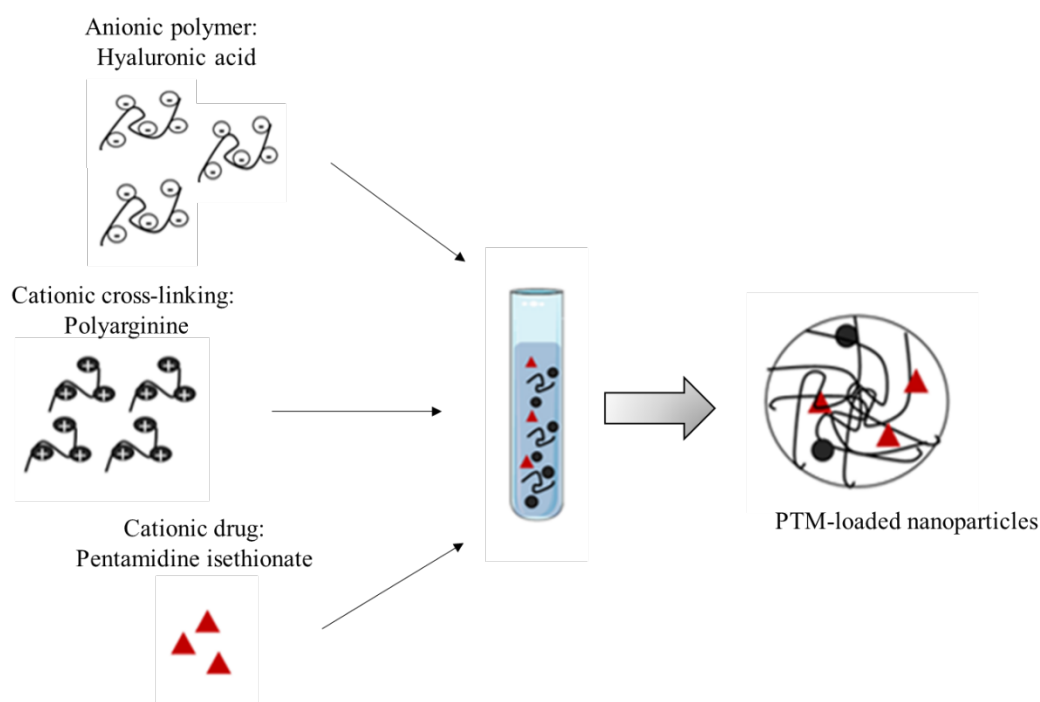


Figure 5. Preparation of PTM-loaded nanoparticles by polyelectrolyte association.

The physicochemical characterizations of NPs obtained using a PTM solution of $0.5 \text{ mg} \cdot \text{mL}^{-1}$ concentration (Table 4) showed an average size between 155 and 203 nm with a low *PdI* (< 0.1) and a negative ζ potential ranging from -24 to -18 mV. Interestingly, the incorporation of the drug into NPs caused a reduction of NPs size compared to blank ones (Table 3). The balance between negatively (HA) and positively (PTM and PArg) charged species was reduced in the case of PTM-loaded NPs as compared to the HA-PArg NPs. Therefore, the attractive force that modulates electrostatic interactions within the complexes determined a “condensation phenomenon” responsible of the reduction of the complex particle size^{35,36}. The ζ potential decreased from -24 to -26 mV for

411 Loaded A to Loaded F, and then increased to -18 mV for Loaded G. The effect of NPs size reduction
 412 has been observed also for other particles suggesting the strong interaction between the drug and the
 413 polymeric chains^{18,23}.

414 Since the formation of NPs, the association of PTM to the polymers causes its encapsulation inside
 415 the particles. Association efficiency AE is equivalent to the widely used encapsulation efficiency EE.
 416 The amounts of associated PTM varied from AE= 26% (Loaded A) to as high as AE= 82% (Loaded
 417 G) upon increasing the HA/PArg mole ratio (Table 4). The highest encapsulation efficiencies were
 418 obtained when the amounts of PTM were low, so that high AE (82% for Loaded G) was correlated
 419 with low loading capacity (12% for Loaded G). Taking together all these results, PTM was efficiently
 420 associated in a HA-PArg NPs at a mole ratio above 2.25 and with a loading capacity ranging from 20
 421 to 10%. This data confirms that the addition of PArg to the system had the advantageous effect of
 422 promoting the association of PTM to the systems.

423
 424 **Table 4.** Physicochemical properties of PTM-loaded NPs obtained using a PTM solution at
 425 0.5 mg·mL⁻¹. *PdI*: polydispersity index; AE (%): association efficiency. Values are given as mean ±
 426 *Sem* (*n* ≥ 3).

	Mass ratio [HA: PArg: PTM]	Mole ratio [HA/PArg +PTM]	Size (nm)	<i>PdI</i>	Zeta potential (mV)	Loading capacity (%)	AE (%)
Loaded A	1.25:0.27:0.75	1.13	155 ±3	< 0.1	-24 ±3	33	26 ±3
Loaded B	1.5:0.27:0.75	1.35	159 ±4	< 0.1	-25 ±2	30	31 ±4
Loaded C	2:0.27:0.75	1.80	191 ±20	< 0.1	-27 ±2	25	46 ±5
Loaded D	2.5:0.27:0.75	2.25	157 ±6	< 0.1	-25 ±5	21	61 ±5
Loaded E	3:0.27:0.75	2.70	172 ±14	< 0.1	-29 ±4	19	65 ±1
Loaded F	3.5:0.27:0.75	3.15	179 ±4	< 0.1	-26 ±1	17	76 ±1
Loaded G	5:0.27:0.75	4.51	203 ± 9	< 0.1	-18 ±1	12	82 ±1

427
 428 The fraction of associated PTM increased as a function of the concentration of HA (from Loaded A
 429 to Loaded G). The highest PTM binding efficiency was obtained for the formulation Loaded F

430 containing 2.3 mg·mL⁻¹ of HA and Loaded G containing 3.3 mg·mL⁻¹ of HA. These results confirmed
431 the ability of NPs to associate a high quantity of PTM by electrostatic interaction. Then, Loaded F
432 and Loaded G were selected for the *in vitro* studies. Previous papers reported the different
433 nanosystems for PTM encapsulation. Encapsulation of PTM inside liposome yielded an association
434 efficiency below 50% due to the hydrophilic character of PTM³⁷. PTM has also been encapsulated
435 into other types polymeric NPs such as PLGA NPs. As described for the liposome formulation, the
436 loading efficiency of PTM was very low (around 2.9%)²⁵.
437 Micale et al. developed PTM-HA bioconjugates in which drug loading ranged from 20 to 30%.
438 However, the use of chemical reactions and organic solvents compromised the direct exploitation of
439 the conjugate for drug delivery applications³⁵.

440

441 **3.5. Quantification of isethionate ions using ion-exchange chromatography**

442 According to electrostatic binding of counterions to polyelectrolytes in solution, the ion concentration
443 in the counterion cloud that surrounds the charged molecules is significantly higher than that in the
444 solution, especially at low ionic strength. Formation of an electrostatic complex of PTM with HA
445 weakens electrostatic binding of isethionate counterions to PTM, so, isethionate counterions are
446 released in bulk solution. The balance is a competitive binding of HA and isethionate to PTM which
447 is shifted towards HA because of its large negative charge (it is a polyelectrolyte) compared to the
448 monovalent isethionate anion. In case of full ion exchange of HA for isethionate, the overall charge
449 of the particles varies as the PTM/HA mole ratio. In the absence of ion exchange (adsorption of the
450 neutral PTM-isethionate ion pair), loading PTM does not change electrostatic phenomena with
451 respect to blank NPs. The balance of isethionate binding to NPs controls the NPs charge, thus the
452 onset of NPs formation. When two opposite charged macro-ions form a complex, as in the case of
453 HA with PTM and PArg, the electrical double layer is perturbed and counterions are released to the
454 bulk solution³⁸. To assess the influence of HA concentration on the formation of PTM-loaded NPs
455 (Loaded B, C, D, E and F), the release of isethionate, the counterion of PTM, was quantified using

ion exchange chromatography. The results show that the full amount of isethionate was released upon formation of all NPs irrespective of the amount of HA. This shows that electrostatic interactions between HA and PTM are predominant. It should be kept in mind that association by strong interactions remains an equilibrium that could be shifted according to changes of external condition (pH, ionic strength).

461

3.6. Morphological analysis of blank and pentamidine-loaded nanoparticles

The morphological analysis of HA-PArg NPs (Blank H and I) and PTM-loaded NPs (Loaded F and G) was carried out using TEM and Cryogenic transmission electron microscopy (CryoTEM). As shown in Figure 6, HA-PArg NPs and PTM-loaded NPs formed monodispersed population of regular rounded-shaped particles as observed by DLS measurements. The addition of the drug did not modify the morphology of the NPs.

Besides, to prepare TEM samples, NPs were stained and dried before the analysis. This preparation step might modify the structure of the NPs. Observation NPs in their native state was achieved with Cryo-TEM. Both measurements showed similar results and confirmed the DLS analysis (Figure 7).

471

472

473

474

475

476

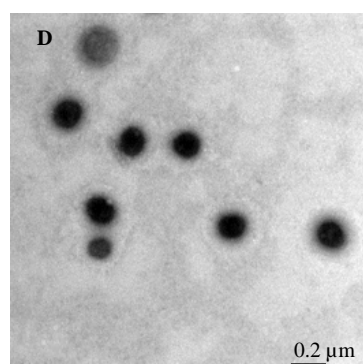
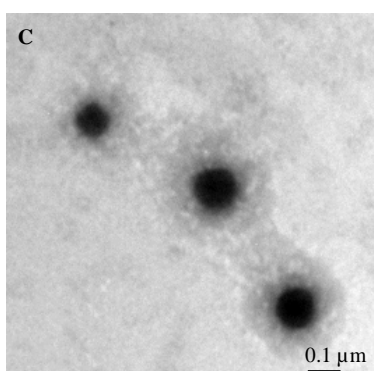
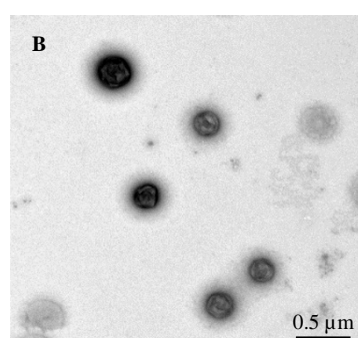
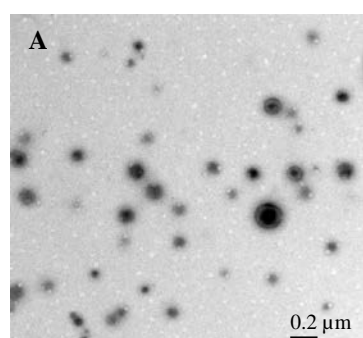
477

478

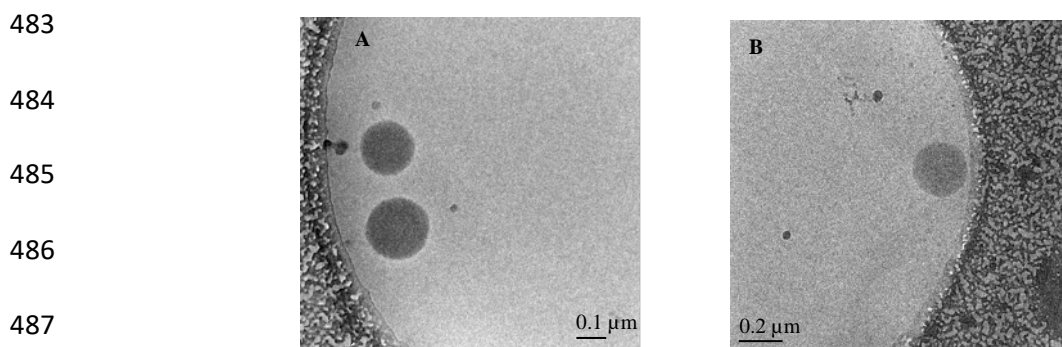
479

480

481



482 **Figure 6.** TEM images of Blank H (A); Blank I (B); Loaded F (C) and Loaded G (D).



488 **Figure 7.** Cryo-TEM images of Loaded F with $2.3 \text{ mg} \cdot \text{mL}^{-1}$ of HA (A) and Loaded G with
489 $3.3 \text{ mg} \cdot \text{mL}^{-1}$ of HA (B).

490

491 **3.7. *In vitro* release study of pentamidine-loaded nanoparticles**

492 The release study has been performed for HA-PArg NPs (loaded F and loaded G) upon incubation
493 with PBS at 37°C using vertical diffusion Franz[®] cells. For both the formulations a biphasic profile
494 release was observed characterized by an initial burst release in the first 10 hours, 6% of release after
495 15 minutes increasing up to 50% after 8 hours, followed by a constant release (see figure 8). This
496 behavior has been described also for others hydrophilic polymer-based NPs³⁹. According to the
497 authors, the encapsulation of a hydrophilic drug allows a quicker penetration of water in the system
498 causing the swelling of polymeric matrix and the formation of pores. The initial burst release is
499 probably due to a fast erosion of the surface that cause the disaggregation of the polymeric matrix
500 with a fast drug release. When the swelling of the matrix is compensated by erosion process a constant
501 release towards water as receptor medium was observed. Moreover, the release behavior of PTM
502 from NPs was similar to the control PTM solution. This shows that the rate-limiting step of the
503 experiment was the diffusion of PTM through the dialysis membrane.

504

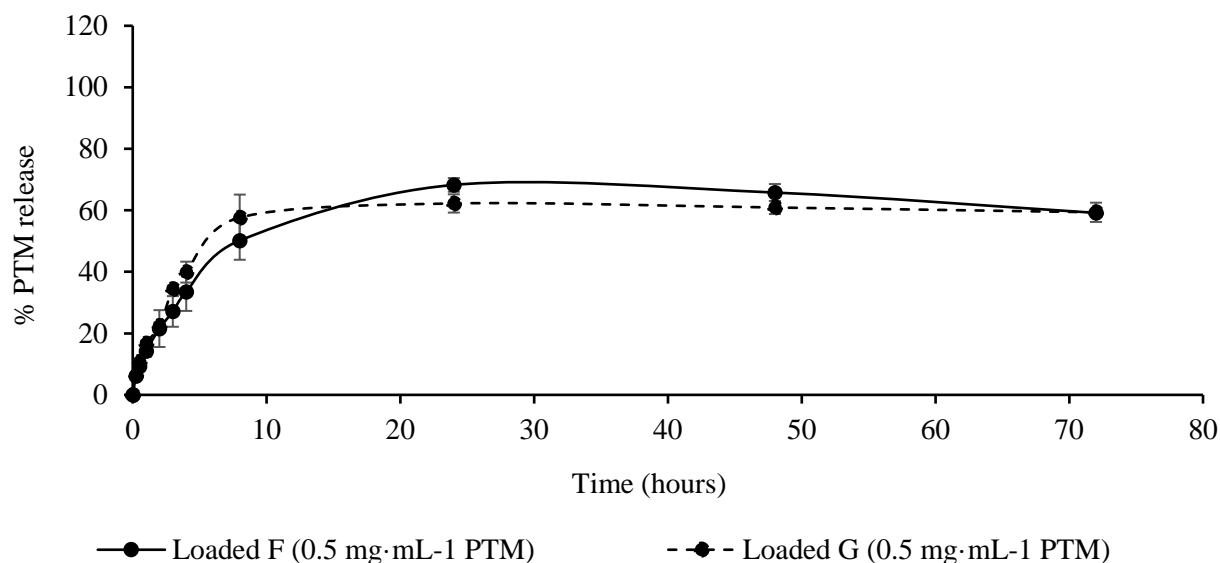


Figure 8. Release profile of PTM from loaded F and loaded G in PBS medium. The diffusion cells were thermoregulated with a water jacket a 37 °C. (Mean \pm S.D.; n = 3).

3.8. Stability studies of blank and pentamidine-loaded nanoparticles

The stability of colloidal suspensions of Blank H and I (Figure 9-A) and Loaded F and G (Figure 9-B) NPs at 4 °C was evaluated over 1 month of storage. Size, polydispersity index and leakage of PTM were evaluated every week. As reported in Figure 8-A and B, size and *PdI* of Blank H and I increased over time for both formulations. However, Blank (H-I) and Loaded NPs (F-G) were more stable cause they were more negative and more stabilized by electrostatic repulsions. No leakage of the drug was observed for both formulations, demonstrating the ability of NPs to associate PTM in an efficient manner. In addition, Blank H and PTM-Loaded F did not aggregate in DMEM (data not shown).

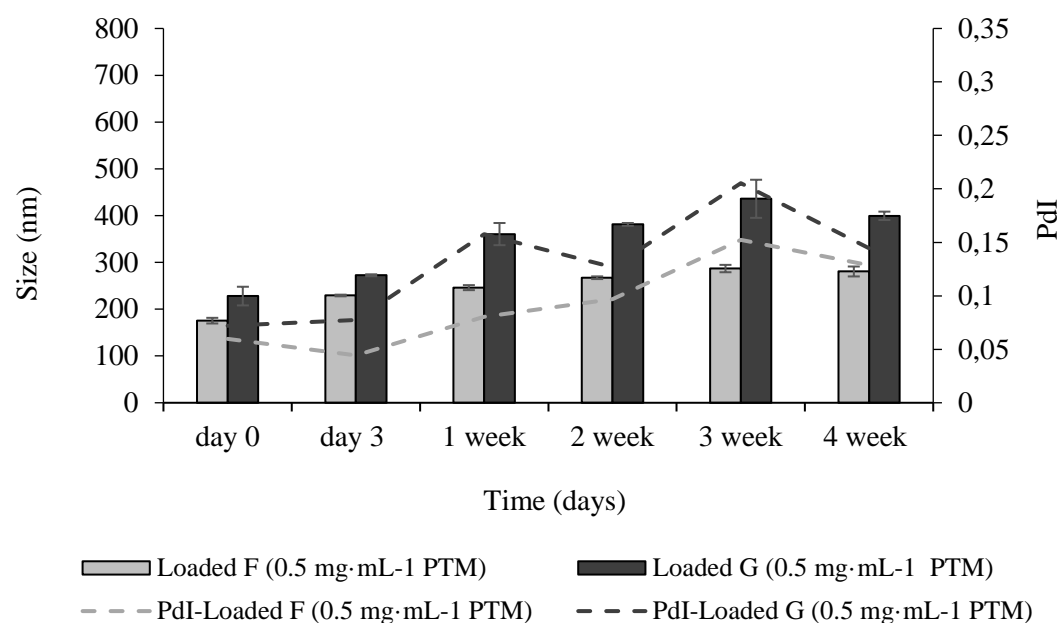
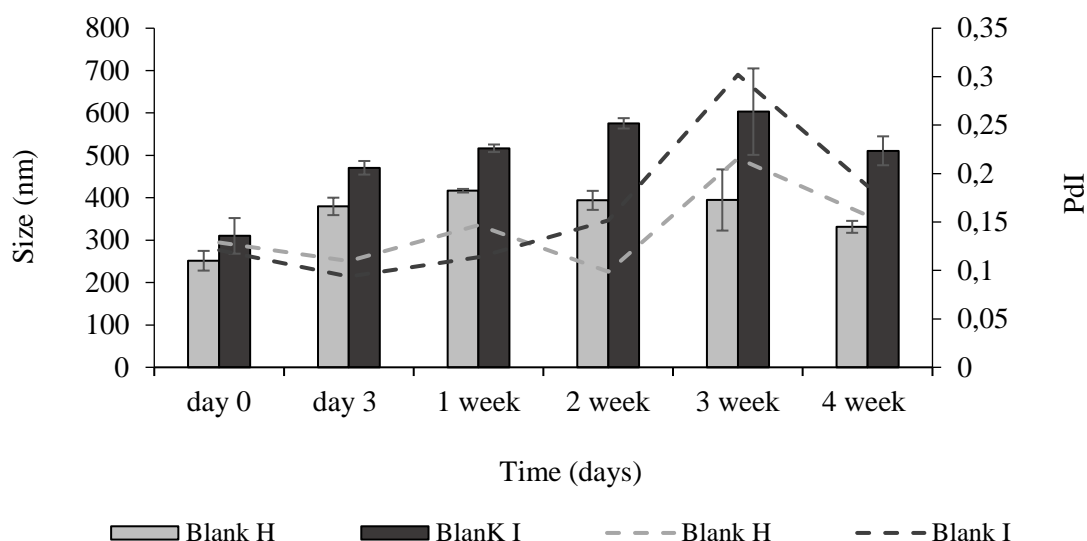


Figure 9. Stability studies, size and *Pdl*, upon storage condition for 4 weeks at 4°C in aqueous solution of Blank H with 3.5 mg·mL⁻¹ of HA, Blank I with 5 mg·mL⁻¹ of HA (A) and Loaded F with 2.3 mg·mL⁻¹ of HA, Loaded G with 3.3 mg·mL⁻¹ of HA (B). *Pdl*: polydispersity index. (Mean ± *Sem*; *n* = 3).

3.9. Freeze-drying studies of blank and pentamidine-loaded nanoparticles

528 A dry form of blank and loaded NPs selected was prepared by freeze-drying in order to study the
 529 long-term stability. The optimal freeze-drying conditions that convert the aqueous suspension into
 530 dry powder and allow for reconstitution in physiological serum were set up. Blank H, Blank I, Loaded
 531 F and Loaded G were freeze-dried using different amount of mannitol (5%, 10% w/v) as bulking and
 532 isotonic agent. The aim was to obtain isotonic values close to physiological condition (280-
 533 300 mOsm·L⁻¹). Tables 5 and 6 show the physiochemical characteristics (size, *PdI* and osmolarity)
 534 of Blank H and Loaded F formulations prepared with different mannitol concentrations, before and
 535 after redispersion in water. Also, stability after redispersion was evaluated over 15 days at 4 °C. Blank
 536 H and Loaded F, were successfully dispersed in water irrespective of the amount of mannitol used.
 537 However, 5% mannitol was needed to obtain isotonic formulation. Following reconstitution in water,
 538 the size of HA-PArg NPs and PTM-loaded NPs increased. Moreover, the size continued to increase
 539 during the storage period for the both formulations (Table 5-6). However, the population remained
 540 monodispersed (*PdI* > 0.1) and no leakage of the drug during the time was observed. **Figure 10**
 541 confirms that both Blank H and Loaded F recovered the initial morphology characteristics upon
 542 freeze-drying and reconstitution in water. Both formulations formed monodispersed population
 543 showing a regular round shape and no aggregation was detected.

544

545 **Table 5.** Physicochemical characterization of Blank H before and after freeze-drying and
 546 reconstitution. *PdI*: polydispersity index. Results are expressed as mean values \pm *Sem*; *n* = 3.

5% mannitol				10% mannitol		
Days	Size (nm)	<i>PdI</i>	Osmol. (mOsm·L ⁻¹)	Size (nm)	<i>PdI</i>	Osmol. (mOsm·L ⁻¹)
0	151 \pm 5	< 0.1	-	148 \pm 6	-	-
0	218 \pm 5	< 0.1	665	210 \pm 8	< 0.1	305
8	233 \pm 7	< 0.1	665	254 \pm 11	< 0.2	305
16	315 \pm 45	< 0.1	665	383 \pm 42	< 0.2	305

547

548 **Table 6.** Physicochemical characterization of Loaded F after freeze-drying and reconstitution. *PdI*:
549 polydispersity index. *AE* (%) association efficiency. Results are expressed as mean values \pm *Sem*; *n*
550 = 3.

5% mannitol					10% mannitol			
Days	Size (nm)	<i>PdI</i>	<i>AE</i> (%)	Osmol. (mOsm·L ⁻¹)	Size (nm)	<i>PdI</i>	<i>AE</i> (%)	Osmol. (mOsm·L ⁻¹)
0	149 \pm 1	< 0.1	79 \pm 1	-	157 \pm 6	-	64 \pm 2	-
0	234 \pm 12	< 0.2	76 \pm 1	669	204 \pm 12	< 0.1	64 \pm 4	297
8	287 \pm 13	< 0.1	-	669	265 \pm 3	< 0.1	-	297
16	353 \pm 6	< 0.1	78 \pm 1	669	321 \pm 10	< 0.2	75 \pm 1	297

551

552

553

554

555

556

557

558

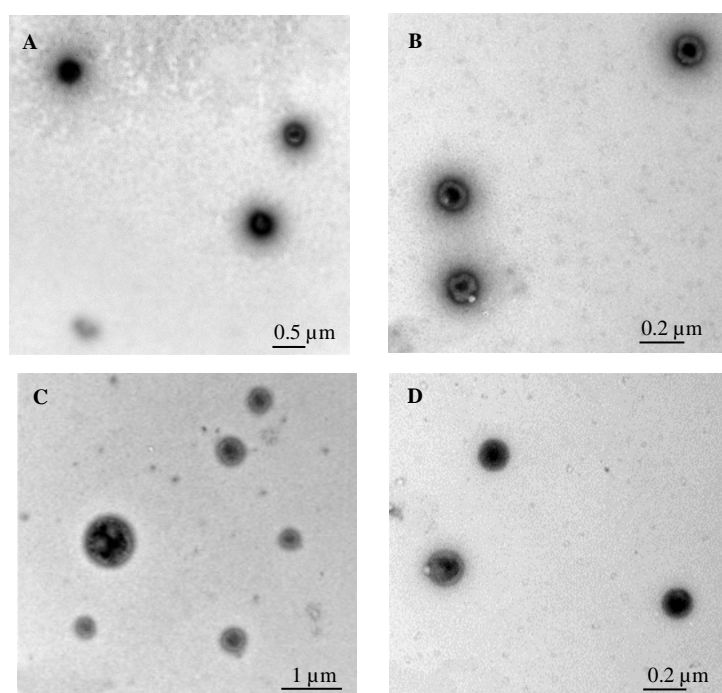
559

560

561

562

563



564 **Figure 10.** TEM pictures of Blank H (A-B) and Loaded F (C-D) nanoparticles after freeze-drying
565 and reconstitution in 1 mL of water.

566

567 3.10. *In vitro* cell viability studies of pentamidine-loaded nanoparticles

568 The antiproliferative activity of free and encapsulated PTM into Loaded F was assessed using the
 569 MTT assay. Lung (A549) and human breast cancer (MDA-MB-231) cell lines were selected based
 570 on their sensitivity to PTM^{24,40}. The viability of A549 and MDA-MB-231 was monitored after
 571 incubation with different concentrations of free PTM and PTM-loaded NPs for 72 h. Blank H were
 572 used as controls to evaluate the biocompatibility of the nanocarrier. As shown in Table 7, the use of
 573 Loaded F was associated with a better activity than free PTM both on lung ($IC_{50} = 0.21 \pm 0.08 \mu M$
 574 vs $1.2 \pm 0.8 \mu M$) and breast cancer cells ($IC_{50} = 2.2 \pm 1.8 \mu M$ vs $4.6 \pm 3.7 \mu M$). Blank I showed very
 575 low toxicity ($IC_{50} > 40 \mu M$) highlighting the biocompatibility of the nanocarrier. These data
 576 confirmed that PTM activity *in vitro* was improved when the drug was incorporated inside
 577 nanoparticles.

578 As reported in the literature both cell lines express CD44 receptors^{41,42}. Hence, we suggest that the
 579 present NPs can target cancer cells *in vivo* through interaction with this receptor.

580 In line with our study, Battistini et al.¹⁷ observed that in A549 cells, cytotoxicity of HA-doxorubicin
 581 complexes was 3-fold higher than that of the reference free drug. These results indicated an increased
 582 cellular uptake of doxorubicin when complexed with HA due to the presence of CD44 membrane
 583 receptors¹⁵.

584 Targeting CD44 using HA moieties has also been demonstrated *in vivo* in CD44-positive human
 585 breast tumor xenografts mice. HA based micelles loaded with paclitaxel exhibit a remarkably high
 586 accumulation and retention in the CD44 receptor-overexpressing tumor following i.v. injection in
 587 comparison to the free drug¹⁶.

588

589 **Table 7.** IC_{50} values of studied compounds on A549 and MDA-MB-231 cells. Results are expressed
 590 as mean values $\pm Sem$; $n = 3$.

Cell line	Formulations	IC_{50} (μM)
	PTM	1.2 ± 0.8

A549	PTM-loaded NPs	0.21 ± 0.08
	Blank HA NPs	42 ± 16
MDA-MB-231	PTM	4.6 ± 3.7
	PTM-loaded NPs	2.2 ± 1.8
	Blank HA NPs	66 ± 47

4. Conclusions

The present study provides insight into a new HA based nano-complex, namely nanoparticles, for encapsulation of positively charged hydrophilic drug. In a first set of experiments, HA-PTM complexes were studied. Such complexes were highly polydispersed species that remained soluble in water. To stabilize the complex and to maximize the amount of the drug associated to the system, HA-PArg NPs were developed using polyelectrolyte complexation technique. NPs were kinetically stabilized by the excess charge, which prevented their aggregation and ensured high encapsulation efficiency of PTM. Also, high encapsulation efficiency was associated to the release of the isethionate counterion in the solution quantified by IC. Following *in vitro* studies, PTM-loaded NPs were more effective in reducing cell viability as compared with free drug suggesting enhanced efficacy and cell internalization via CD44 receptor. Moreover, their optimum pharmaceutical properties, namely easy production using mild conditions, stability and possibility to obtain ready-to-use dry powders, highlight the potential of HA-PArg nanoparticles as novel drug delivery system for nanomedicine applications.

Funding Sources

This work has been carried out within the research program RESOLVE, financially supported by EuroNanoMed-III (8th call). Flavia Carton had a fellowship from the Ministry of Education of Italy. The research leading to these results has received funding from Italian Ministry for University and Research (MIUR)-University of Torino, “Fondi Ricerca Locale (ex-60%)”.

612

613 **Notes**

614 The authors declare no competing financial interests.

615

616 **Acknowledgements**

617 Authors are thankful to Geraldine Agusti, Sébastien Urbaniak from University of Lyon 1, CNRS,
618 LAGEPP UMR 5007, for their kind help with TEM images and lyophilization studies. We would like
619 to acknowledge the contribution of Pierre-Yves Dugas (University of Lyon 1, C2P2 UMR 5265) for
620 cryo-TEM observations at the “Centre Technologique des Microstructures” (CT μ - University of
621 Lyon 1). Emeline Perrial and Zineb Bousfiha from CRCL, are gratefully acknowledged for cell
622 culture.

623 **References**

- 624 1. Marras A, Vieregg J, Ting J, Rubien J, Tirrell M. Polyelectrolyte Complexation of
625 Oligonucleotides by Charged Hydrophobic – Neutral Hydrophilic Block Polymers. *Polymers*.
626 2019; 11,83.
- 627 2. Myung GK, Sung DJ, Ji HJ, Sun HK. Nanoscale polyelectrolyte complexes encapsulating
628 mRNA and long-chained siRNA for combinatorial cancer gene therapy. *J Ind and end chem*.
629 2018; 64:430-437.
- 630 3. Joshi JR, Patel RP. Role of biodegradable polymers in drug delivery. *Int J Curr Pharm Res*.
631 2012;4:74-81.
- 632 4. Goycoolea FM, Lollo G, Remuñán-López C, Quaglia F, Alonso MJ. Chitosan-alginate blended
633 nanoparticles as carriers for the transmucosal delivery of macromolecules.
634 *Biomacromolecules*. 2009;10:1736-1743.
- 635 5. Pistone S, Goycoolea FM, Young A, Smistad G, Hiorth M. Formulation of polysaccharide-
636 based nanoparticles for local administration into the oral cavity. *Eur J Pharm Sci*. 2017;96:381-
637 389.
- 638 6. Weber C, Drogoz A, David L, Domard A, Charles MH, Verrier B, Delair T. Polysaccharide-
639 based vaccine delivery systems: Macromolecular assembly, interactions with antigen
640 presenting cells, and in vivo immunomonitoring. *J Biomed Mater Res - Part A*. 2010;93:1322-
641 1334.
- 642 7. Liu Z, Jiao Y, Wang Y, Zhou C, Zhang Z. Polysaccharides-based nanoparticles as drug
643 delivery systems. *Adv Drug Deliv Rev*. 2008;60:1650-1662.
- 644 8. Morra M. Engineering of biomaterials surfaces by hyaluronan. *Biomacromolecules*.
645 2005;6:1205-1223.

- 646 9. Dosio F, Arpicco S, Stella B, Fattal E. Hyaluronic acid for anticancer drug and nucleic acid
647 delivery. *Adv Drug Deliv Rev.* 2016;97:204-236.
- 648 10. Chen B, Miller RJ, Dhal PK. Hyaluronic acid-based drug conjugates: State-of-the-art and
649 perspectives. *J Biomed Nanotechnol.* 2014;10:4-16.
- 650 11. Cadete A. Targeting cancer with hyaluronic acid-based nanocarriers: recent advances and
651 translational perspectives. *Nanomedicine.* 2016;11:2341-2357.
- 652 12. Lee GY, Kim J-H, Choi KY, Yoon HY, Kim K, Kwon IC, Choi K, Lee B-H, Park JH, Kim I-
653 S. Hyaluronic acid nanoparticles for active targeting atherosclerosis. *Biomaterials.*
654 2015;53:341-348.
- 655 13. ~~Mero A. and Campisi M. Hyaluronic Acid Bioconjugate for the Delivery of Bioactive~~
656 ~~Molecules. *Polymers.* 2014; 6:346-369.~~
- 657 14. ~~Misra S., Hascall V.C., Markwald R.R., Ghatak S. Interactions between hyaluronan and its~~
658 ~~receptors (CD44, RHAMM) regulate the activities of inflammation and cancer. *Front Immunol.*~~
659 ~~2015; 6:201.~~
- 660 15. Battistini FD, Flores-Martin J, Olivera ME, Genti-Raimondi S, Manzo RH. Hyaluronan as
661 drug carrier. The in vitro efficacy and selectivity of Hyaluronan-Doxorubicin complexes to
662 affect the viability of overexpressing CD44 receptor cells. *Eur J Pharm Sci.* 2014;65:122-129.
- 663 16. Zhong Y, Goltsche K, Cheng L, [Xie F](#), [Meng F](#), [Deng C](#), [Zhong Z](#), [Haag R](#). Hyaluronic acid-
664 shelled acid-activatable paclitaxel prodrug micelles effectively target and treat CD44-
665 overexpressing human breast tumor xenografts in vivo. *Biomaterials.* 2016;84:250-261.
- 666 17. Battistini FD, Olivera ME, Manzo RH. Equilibrium and release properties of hyaluronic acid-
667 drug complexes. *Eur J Pharm Sci.* 2013;49:588-594.
- 668 18. Thomas RG, Moon MJ, Lee SJ, Jeong YY. Paclitaxel loaded hyaluronic acid nanoparticles for

- 669 targeted cancer therapy: In vitro and in vivo analysis. *Int J Biol Macromol*. 2014;72:510-518.
- 670 19. Choi KY, Chung H, Min KH, Yoon HY, Kim K, Park JH, Kwon IC, Jeong SY. Self-assembled
671 hyaluronic acid nanoparticles for active tumor targeting. *Biomaterials*. 2010;31:106-114.
- 672 20. Lin C, Kim SB, Yon J-M, Park SG, Gwon LW, Lee J-G, Baek I-J, Lee BJ, Yun YW, Nam S-
673 Y. Temporal and subcellular distributions of Cy5.5-labeled hyaluronic acid nanoparticles in
674 mouse organs during 28 days as a drug carrier. *Korean J Vet Res*. 2017;57:215-222.
- 675 21. Nagavarma BVN, Yadav HKS, Ayaz A, Vasudha LS, Shivakumar HG. Different techniques
676 for preparation of polymeric nanoparticles - A review. *Asian J Pharm Clin Res*. 2012;5(Suppl.
677 3):16-23.
- 678 22. Contreras-Ruiz L, de la Fuente M, Párraga JE, López-García A, Fernández I, Seijo B, Sánchez
679 A, Calonge M, Diebold Y. Intracellular trafficking of hyaluronic acid-chitosan oligomer-based
680 nanoparticles in cultured human ocular surface cells. *Mol Vis*. 2011;17:279-290.
- 681 23. Lollo G, Benoit JP, Brachet M, Drug delivery system, European Patent
682 Office(EP18306201.7)2018, Pending licence.
- 683 24. Jung HJ, Suh S Il, Suh MH, Baek WK, Park JW. Pentamidine reduces expression of hypoxia-
684 inducible factor-1 α in DU145 and MDA-MB-231 cancer cells. *Cancer Lett*. 2011;303:39-46.
- 685 25. Arias JL, Unciti-Broceta JD, Maceira J, del Castillo T, Hernández-Quero J, Magez S, Soriano
686 M, García-Salcedo JA. Nanobody conjugated PLGA nanoparticles for active targeting of
687 African Trypanosomiasis. *J Control Release*. 2015;197:190-198.
- 688 26. Lollo G, Gonzalez-Paredes A, Garcia-Fuentes M, Calvo P, Torres D, Alonso MJ. Polyarginine
689 nanocapsules as a potential oral peptide delivery carrier. *J Pharm Sci*. 2017;106:611-618.
- 690 27. Wang S, Cao M, Deng X, Xiao X, Yin Z, Hu Q, Zhou Z, Zhang F, Zhang R, Wu Y, Sheng W,
691 Zeng Y. Degradable hyaluronic acid/protamine sulfate interpolyelectrolyte complexes as

- 692 miRNA-delivery nanocapsules for triple-negative breast cancer therapy. *Adv Healthc Mater.*
693 2015;4:281-90.
- 694 28. ~~Teijeiro Valiño C, Yebra Pimentel E, Guerra Varela J, Csaba N, Alonso MJ, Sánchez L.~~
695 ~~Assessment of the permeability and toxicity of polymeric nanocapsules using the zebrafish~~
696 ~~model. *Nanomedicine.* 2017;12:2069-2082.~~
- 697 29. Oyarzun-Ampuero FA, Goycoolea FM, Torres D, Alonso MJ. A new drug nanocarrier
698 consisting of polyarginine and hyaluronic acid. *Eur J Pharm Biopharm.* 2011;79:54-57.
- 699 30. Dautzenberg H. Polyelectrolyte complex formation in highly aggregating systems. 1. Effect of
700 salt: Polyelectrolyte complex formation in the presence of NaCl. *Macromolecules.*
701 1997;30:7810-7815.
- 702 31. Doderio A, Williams R, Gagliardi S, Vicini S, Alloisio M, Castellano M. Characterization of
703 hyaluronic acid by dynamic light scattering and rheological techniques. *AIP Conf Proc.*
704 2018;1981:020184-1-020184-4.
- 705 32. Maleki A, Kjøniksen AL, Nyström B. Effect of pH on the behavior of hyaluronic acid in dilute
706 and semidilute aqueous solutions. *Macromol Symp.* 2008;274:131-140.
- 707 33. Nyström B, Lindman B. Dynamic and viscoelastic properties during the thermal gelation
708 process of a nonionic cellulose ether dissolved in water in the presence of ionic surfactants.
709 *Macromolecules.* 1995;28(4):967-974.
- 710 34. Maleki A, Kjøniksen AL, Knudsen KD, Nyström B. Dynamical and structural behavior of
711 hydroxyethylcellulose hydrogels obtained by chemical gelation. *Polym Int.* 2006;55:365.
- 712 35. Micale N, Piperno A, Mahfoudh N, Schurigt U, Schultheis M, Mineo PG, Schirmeister T,
713 Scala A, Grassi G. A hyaluronic acid-pentamidine bioconjugate as a macrophage mediated
714 drug targeting delivery system for the treatment of leishmaniasis. *RSC Adv.* 2015;5:95545-

715 95550.

716 36. Paul M, Durand R, Boulard Y, Fusai T, Fernandez C, Rivollet D, Deniau M, Astier A.
717 Physicochemical characteristics of pentamidine-loaded polymethacrylate nanoparticles:
718 Implication in the intracellular drug release in *Leishmania major* infected mice. *J Drug Target*.
719 1998;5:481-490.

720 37. Mérian J, De Souza R, Dou Y, Ekdawi SN, Ravenelle F, Allen C. Development of a liposome
721 formulation for improved biodistribution and tumor accumulation of pentamidine for oncology
722 applications. *Int J Pharm*. 2015;488:154-164.

723 38. Van der Guch J, Spruijt E, Lemmers M, Coen Stuart MA. Polyelectrolyte complexes: Bulk
724 phases and colloidal systems, *J Colloid Interface Sci*. 2011;361:407-422.

725 39. Chakraborty S1, Khandai M, Sharma A, Patra ChN, Patro VJ, Sen KK. Effects of drug
726 solubility on the release kinetics of water soluble and insoluble drugs from HPMC based matrix
727 formulations. *Acta. Pharm*. 2009; 59:313-323.

728 40. Lee MS, Johansen L, Zhang Y, Wilson A, Keegan M, Avery W, Elliott P, Borisy AA, Keith
729 CT. The novel combination of chlorpromazine and pentamidine exerts synergistic
730 antiproliferative effects through dual mitotic action. *Cancer Res*. 2007;67:11359-11368.

731 41. Olsson E, Honeth G, Bendahl PO, Saal LH, Gruvberger-Saal S, Ringnér M, Vallon-Christersson
732 J, Jönsson G, Holm K, Lövgren K, Fernö M, Grabau D, Borg A, Hegardt C. CD44 isoforms
733 are heterogeneously expressed in breast cancer and correlate with tumor subtypes and cancer
734 stem cell markers. *BMC Cancer*. 2011;11:418.

735 42. Jeannot V, Mazzaferro S, Lavaud J, Vanwonderghem L, Henry M, Arboléas M, Vollaie J,
736 Josserand V, Coll JL, Lecommandoux S, Schatz C, Hurbin A. Targeting CD44 receptor-positive
737 lung tumors using polysaccharide-based nanocarriers: Influence of nanoparticle size and
738 administration route. *Nanomedicine*. 2016; 12(4):921-932.

739

740